

## AC conductivity and dielectric properties of $\text{Co}_{0.5}\text{Zn}_{0.5}\text{Fe}_2\text{O}_4$ nanoparticles disk

M. I. M. Ismail<sup>\*1,2</sup>, Eman Elesh<sup>1</sup>

<sup>1</sup> Department of Physics, Faculty of Science/ Port Said University, Port Said, Egypt

<sup>2</sup> Department of Physics, Faculty of Arts and Science in Almikhwah/ AlBaha University, Almikhwah, Saudi Arabia

Corresponding Author: M. I. M. Ismail

---

**Abstract:** The powder exhibits a polycrystalline structure with cubic system. The topography for  $\text{Co}_{0.5}\text{Zn}_{0.5}\text{Fe}_2\text{O}_4$  depicts that the particles have granular shape with crystalline nature with average of particle size 11.58 nm. The electrical conductivity and dielectric properties of the  $\text{Co}_{0.5}\text{Zn}_{0.5}\text{Fe}_2\text{O}_4$  has been investigated. The correlated barrier hopping (CBH) modulus has been applied to the interpretation of the AC electrical conductivity. Both parts of complex dielectric modulus were investigated.

**Keywords:** Nanoparticles; AC conductivity; dielectric properties; Ferrites.

---

Date of Submission: 12-08-2017

Date of acceptance: 25-08-2017

---

### I. Introduction

Over the last few decades the interest towards soft magnetic materials has increased due to increasing interest for improved of electromagnetic applications such as memory, data storage devices, switching devices and many others [1]. Ferrites are known magnetic materials which have electrical and magnetic properties [2]. Studies of electric and dielectric behavior are equally important for an applied point of view. Polycrystalline ferrites are good dielectric, they have the high permeability and low electrical conductivity which is useful for many technological applications ranging from microwave to radio frequencies [3]. The ferrites have shown to exhibit interesting electrical and dielectric properties in nanoform as compared to the bulk, electrical are mostly controlled by grain boundaries counterpart. The dielectric loss of nanocrystalline is less than the bulk ferrites [4]. The frequency dependent dielectric behavior gives valuable information about localized charge carriers and many physical and chemical properties [5-6]. The application of dielectric and the AC conductivity is the capacitive element in electronic circuits [7]. The preparation method and sintering condition influences the dielectric and magnetic behavior of ferrites [4]. In this research the ferrite was prepared in disk form and the AC electrical conductivity and dielectric properties were investigated.

### II. Experimental Details

#### 2.1 Synthesis of $\text{Co}_{0.5}\text{Zn}_{0.5}\text{Fe}_2\text{O}_4$ Nanoparticles

Ultra fine particles of  $\text{Co}_{0.5}\text{Zn}_{0.5}\text{Fe}_2\text{O}_4$  were prepared by co-precipitating technique, where mixture of 40 ml  $\text{ZnCl}_2$  1M, 40 ml  $\text{CoSO}_4 \cdot 7\text{H}_2\text{O}$  1M and 241.6 ml  $\text{FeCl}_3$  1M was poured to 1100 ml NaOH 1.1 M at room temperature under vigorous stirring. Raise temperature to 100 °C, keep solution to boil under stirring for 1.5 h, after cooling, particles of  $\text{Co}_{0.5}\text{Zn}_{0.5}\text{Fe}_2\text{O}_4$  were washed several times by distilled water till Ph reaches 7.  $\text{Co}_{0.5}\text{Zn}_{0.5}\text{Fe}_2\text{O}_4$  nanoparticles were separated by sedimentation then dried at 80 °C for 4 hours. The dried nanoparticles were grinding to be in the powder form.

#### 2.2 Formation of $\text{Co}_{0.5}\text{Zn}_{0.5}\text{Fe}_2\text{O}_4$ Disc

Suitable amount of  $\text{Co}_{0.5}\text{Zn}_{0.5}\text{Fe}_2\text{O}_4$  nanopowder was pressed by uniaxial press with steel holder with applied pressure 4 bar of model. The  $\text{Co}_{0.5}\text{Zn}_{0.5}\text{Fe}_2\text{O}_4$  pellet has thickness equal 0.266 cm and average diameter of 100 cm<sup>2</sup>.

#### 2.3 Characterizations of $\text{Co}_{0.5}\text{Zn}_{0.5}\text{Fe}_2\text{O}_4$ Nanoparticles

The crystalline structure and grain size were investigated by using X-ray diffraction and Transmission electron microscope (TEM). The structural characteristics of  $\text{Co}_{0.5}\text{Zn}_{0.5}\text{Fe}_2\text{O}_4$  powder were investigated by using a Philips X-ray diffractometer (model X' pert) with utilized monochromatic  $\text{CuK}_\alpha$  radiation ( $\lambda = 1.5418 \text{ \AA}$ ) and operated at 50 kV and 40 mA. The surface morphology for CuTPP thin films was investigated by JEOL-JXA810 electron microscope. The AC conductivity of  $\text{Co}_{0.5}\text{Zn}_{0.5}\text{Fe}_2\text{O}_4$  disc was carried out by using RCL BIRDGE MODEL HIOKI 3532 HITESTER, in frequency range (100-5MHz). The total conductivity,  $\sigma_T(w)$ , is calculated over the temperature range of 303-453 K.

### III. Results And Discussion

#### 3.1 X-Ray Diffraction Analysis

Fig. 1 Shows the X-ray diffraction patterns of the dried  $\text{Co}_{0.5}\text{Zn}_{0.5}\text{Fe}_2\text{O}_4$  nanosample. The diffraction peaks sites and intensity are matching with the standard pattern for JCPDS Cards No. Cards (22-1086 for  $\text{CoFe}_2\text{O}_4$  and 01-1109 for  $\text{ZnFe}_2\text{O}_4$ ).  $\text{Co}_{0.5}\text{Zn}_{0.5}\text{Fe}_2\text{O}_4$  has very broad peaks, indicating the ultra-fine nature and small crystallite size of the particles. Spinel cubic structure of single-phase nano-sized  $\text{Co}_{0.5}\text{Zn}_{0.5}\text{Fe}_2\text{O}_4$  powder has confirmed by the characteristic diffraction lines (220), (311), (400), (422), (511), (440), (620) and (533). According to the Debye–Scherrer formula, the crystallite size  $D_{hkl}$  for the sample is given by [8-10].

$$D_{hkl} = 0.9\lambda/\beta\cos\theta \quad (1)$$

where  $\beta$  is the full-width at half-maximum (FWHM) value of XRD diffraction lines (see Fig. 1), the wavelength  $\lambda = 0.15418$  nm and  $\theta$  is the half diffraction angle of  $2\theta$ . The Particle sizes were determined at the peak  $D_{311}$  for the dried samples. See Table 1.

The particle size is determined by taking the average of the sizes at the peaks  $D_{220}$ ,  $D_{311}$ ,  $D_{400}$ ,  $D_{422}$ ,  $D_{511}$  and  $D_{440}$ . It was found to be 11.58 nm. The lattice parameter " $a_0$ " is determined by eq. (3) Bragg's law (Eq. (2)) [11]. The values obtained are shown in Table 1:

$$d_{hkl} = \frac{\lambda}{2 \sin\theta} \quad (2)$$

$$d_{hkl} = \frac{a}{\sqrt{h^2 + k^2 + l^2}} \quad (3)$$

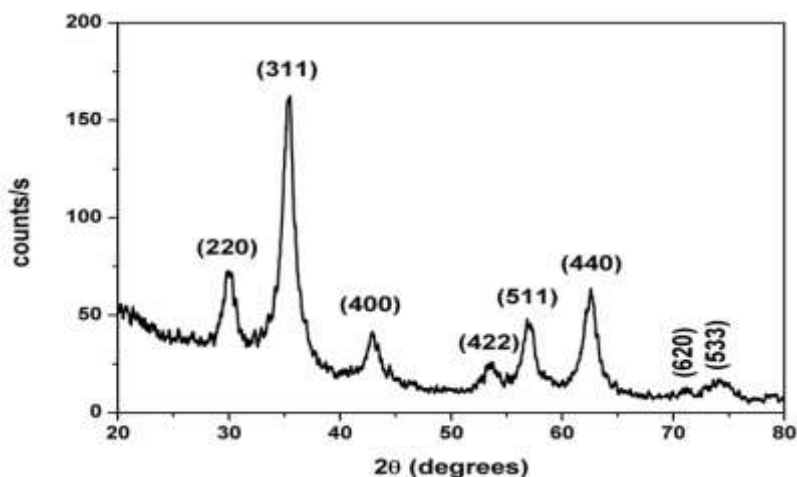


Fig. 1. X-ray diffraction pattern of the dried  $\text{Co}_{0.5}\text{Zn}_{0.5}\text{Fe}_2\text{O}_4$  nanosample.

Fig 2. shows the plotting  $\sqrt{h^2 + k^2 + l^2}$  as a function of  $1/d_{hkl}$ , the lattice parameters " $a_0$ " are calculated by tacking the slope of the curve of fig 2. The goodness of the fit of the data to the formula for the sample is determined by the correlation coefficient ( $R^2 = 1$  is for the perfect fit) which in our case 0.999.

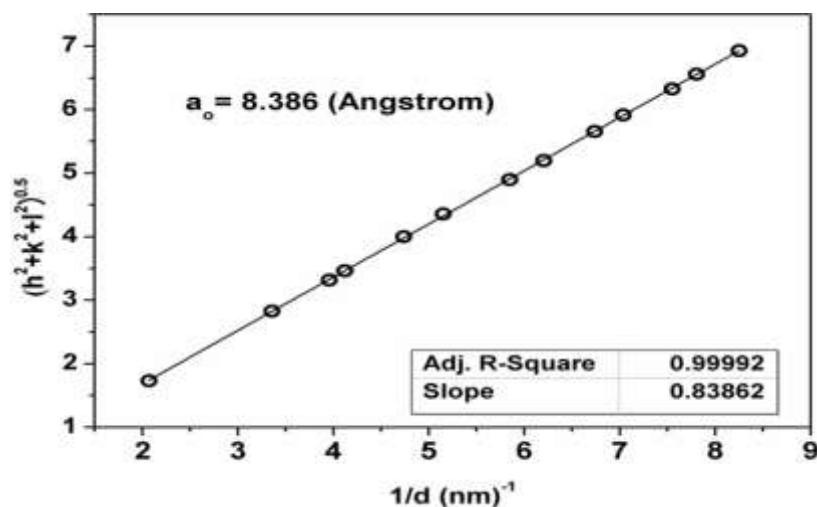


Fig. 2.  $\sqrt{h^2 + k^2 + l^2}$  vs  $(1/d)$  of the dried  $\text{Co}_{0.5}\text{Zn}_{0.5}\text{Fe}_2\text{O}_4$  nanosample.

The lattice parameter for the prepared sample is much closer to the values reported for JCPDS Cards No. Cards (22-1086 for  $\text{CoFe}_2\text{O}_4$  ( $a_0 = 8.3919$ ) and **01-1109** for  $\text{ZnFe}_2\text{O}_4$  ( $a_0 = 8.4030$ )).

Using Williamsone-Hall method, both particle size and lattice strain can calculate by eq. (4) [12]

$$\beta \cos \theta = \frac{k\lambda}{D} + 4\epsilon \sin \theta \tag{4}$$

where  $\beta$  is a measurement of FWHM in radians,  $\theta$  is Bragg angle of the diffraction peaks,  $\lambda$  is the wavelength of the X-rays used,  $D$  is the effective particle size and  $\epsilon$  is the amount of strain [13].

Fig. 3 shows the variation of  $(\beta \cos \theta)$  with  $(4\sin \theta)$  for the  $\text{Co}_{0.5}\text{Zn}_{0.5}\text{Fe}_2\text{O}_4$  sample. Accordingly, the slope and y-intersect of the fitted line represent strain and particle size, respectively. The plots showed a negative strain for the  $\text{Co}_{0.5}\text{Zn}_{0.5}\text{Fe}_2\text{O}_4$  nanopaticles. This negative strain may be due to the lattice shrinkage that was observed in the calculation of lattice parameters. The calculated particle size from Williamsone-Hall method is much closed to the calculated particle size from Debye–Scherrer formula, see table 1.

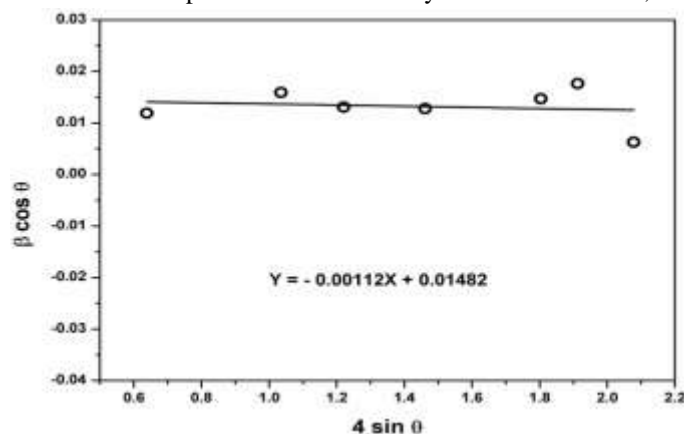


**Fig. 3.** The W-H analysis of dried  $\text{Co}_{0.5}\text{Zn}_{0.5}\text{Fe}_2\text{O}_4$  nanosample assuming UDM. Fit to the data, the strain is extracted from the slope and the crystalline size is extracted from the y-intercept of the fit.

**Table 1:** Geometric parameters of  $\text{Co}_{0.5}\text{Zn}_{0.5}\text{Fe}_2\text{O}_4$  nanoparticles.

Sample	Lattice parameter " $a_0$ " (Å)	averaging the particle size estimated from			
		Scherrer Method	WilliamsoneHall methods		TEM
		D (nm)	D (nm)	$\epsilon$ no Unit x $10^{-3}$	D (nm)
$\text{Zn}_{0.5}\text{Co}_{0.5}\text{Fe}_2\text{O}_4$	8.386	11.58	9.25	1.12	9.5 ±2

### 3.2 Transmission Electron Microscope Studies

High-resolution transmission electron microscopy was used to study the morphology of  $\text{Co}_{0.5}\text{Zn}_{0.5}\text{Fe}_2\text{O}_4$  nanoparticles. The micrograph of  $\text{Co}_{0.5}\text{Zn}_{0.5}\text{Fe}_2\text{O}_4$  is given in Fig. 4. It is cleared that the tested particles are spherical in shape with a narrow size distribution, with a smooth surface and their particle sizes are  $9.5 \pm 2$  nm which is approximately the size calculated by both Debye–Scherrer formula and Williamsone-Hall method. Fig 5. shows a selected area electronic diffraction (SAED) pattern of the nanoparticles and indexed diffraction pattern confirm the crystal planes of  $\text{Co}_{0.5}\text{Zn}_{0.5}\text{Fe}_2\text{O}_4$ .

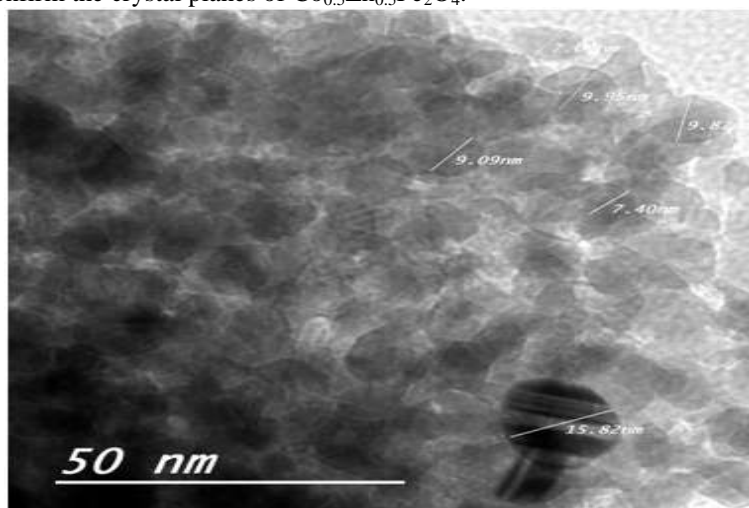


**Fig. 4.** TEM micrograph of the dried  $\text{Co}_{0.5}\text{Zn}_{0.5}\text{Fe}_2\text{O}_4$  nanosample.

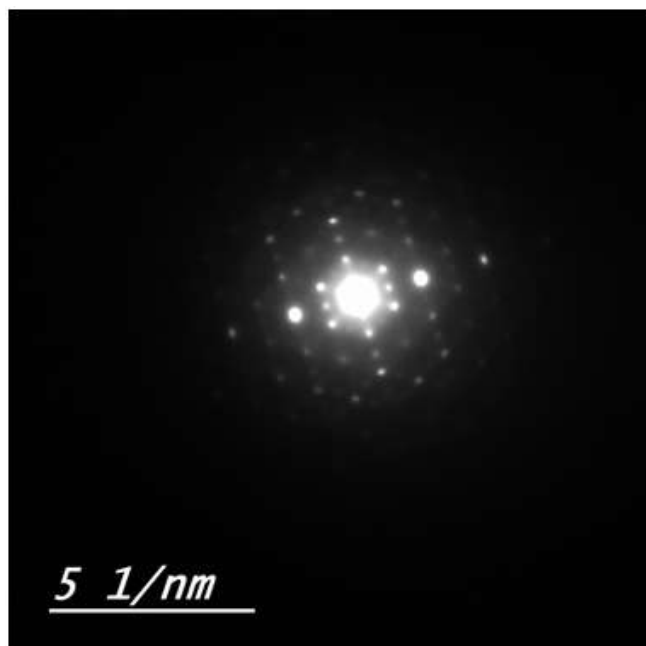


Fig. 5. HRTEM image, SAED pattern of the dried  $\text{Co}_{0.5}\text{Zn}_{0.5}\text{Fe}_2\text{O}_4$  nanosample.

### 3.3 AC Conductivity Measurement and Dielectric Properties of $\text{Co}_{0.5}\text{Zn}_{0.5}\text{Fe}_2\text{O}_4$ Disk

The total conductivity,  $\sigma_{tot}(\omega)$ , as a function of applied frequency in the range of temperature (303-363K) is shown in Fig.6. It can be noticed that the total conductivity tend to increase with increasing the frequency. The AC conductivity,  $\sigma_{AC}(\omega)$ , takes the same behavior with the frequency as shown in Fig.7. The frequency dependence of AC conductivity is characterized by Jonschers power law which described by [14]

$$\sigma_{AC} = A\omega^s \quad (5)$$

where  $A$  is a temperature-dependent constant,  $\omega$  is the angular frequency and  $s$  is the frequency exponent whose value is in range  $0 < s < 1$ ,  $s$  is slope of the straight lines at high frequency region of Fig.7. On the basis of the value of the exponent  $s$ , the correlated barrier hopping (CBH) model describes charge carrier hopping between sites over the potential barrier separating them [15]. In Fig. 8 the values of,  $s$ , were found to decrease from 0.54 to 0.46 with increasing temperature from 303 K to 363K. This result supports that correlated barrier hopping model is the most suitable model to describe the AC electrical conduction for in the desired temperature range. A plot of  $(1-s)$  versus temperature results in a straight line as shown in Fig.9 according to the following equation [16]:

$$s = 1 - \frac{6k_B T}{W_m} \quad (6)$$

where  $W_m$  is the maximum barrier height for hopping at infinite separation. The optional barrier  $W_m$  has been calculated from the slope as 0.4 eV.

Fig.10 shows the variation of the  $\sigma_{AC}(\omega)$  with the reciprocal of temperature for  $\text{Co}_{0.5}\text{Zn}_{0.5}\text{Fe}_2\text{O}_4$ . From the figure,  $\sigma_{AC}(\omega)$  increase linearly by increasing temperature. The temperature dependence of  $\sigma_{ac}(\omega)$  is represented by Mott [17]:

$$\sigma_{ac}(\omega) = \sigma_0 \exp\left(-\frac{\Delta E_{ac}}{kT}\right) \quad (7)$$

where  $\sigma_0$  is a constant and  $\Delta E_{ac}$  is activation energy for conduction. The values of the AC activation energy for the selected frequencies were calculated from the slope, and the values were found decreased as the frequency was increased as shown in fig. 11. It means that the increase of the applied frequency enhances the electronic jump between the localized states [18].

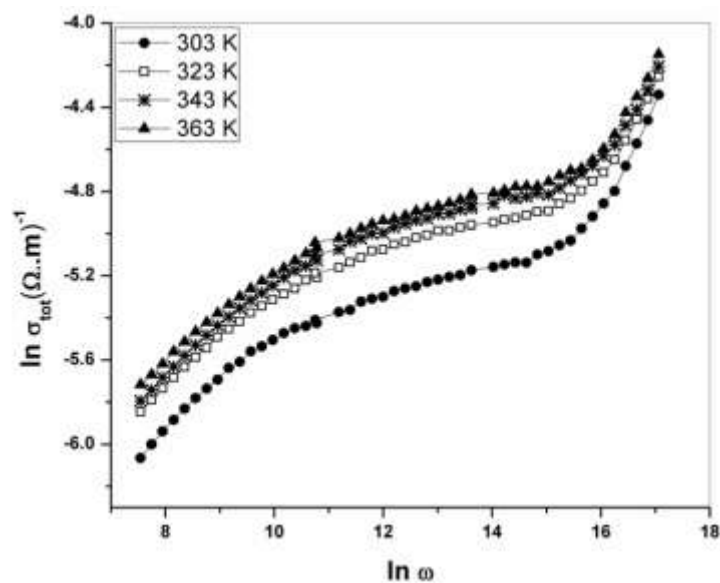


Fig. 6. Frequency dependence of total conductivity at different temperature of  $\text{Co}_{0.5}\text{Zn}_{0.5}\text{Fe}_2\text{O}_4$  disk in range of temperatures (303-363K).

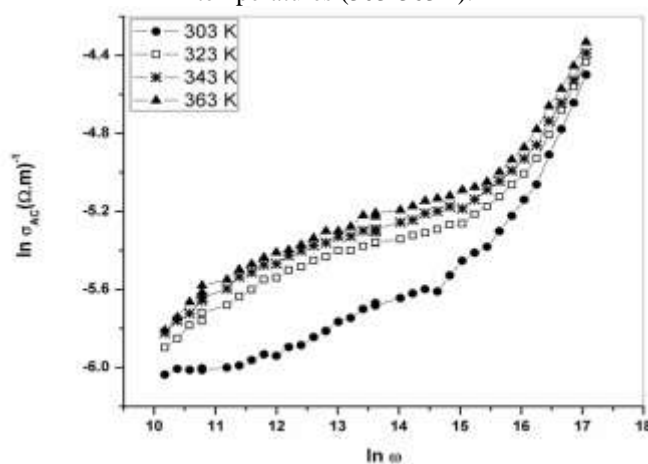


Fig. 7. Frequency dependence of AC conductivity at different temperature of  $\text{Co}_{0.5}\text{Zn}_{0.5}\text{Fe}_2\text{O}_4$  disk in range of temperatures (303-363K).

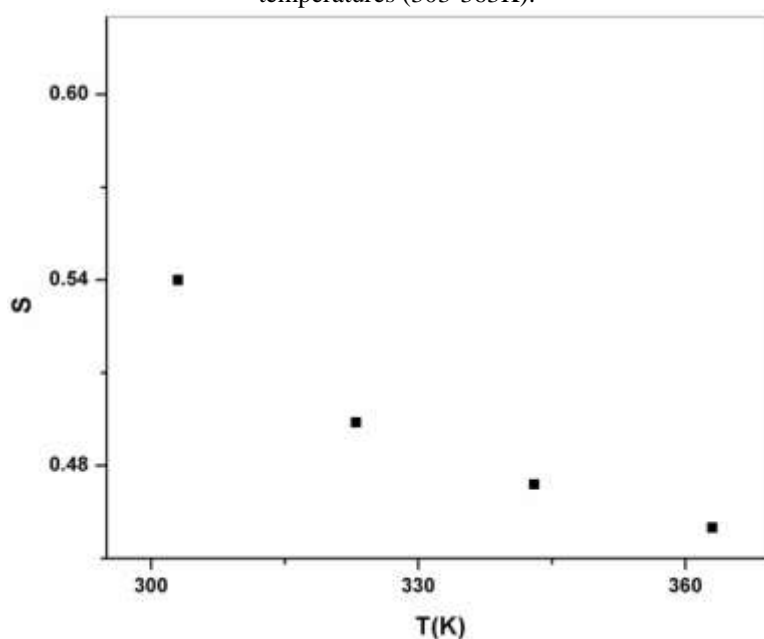


Fig. 8. Temperature dependence of exponent factor of  $\text{Co}_{0.5}\text{Zn}_{0.5}\text{Fe}_2\text{O}_4$  disk at different temperature.

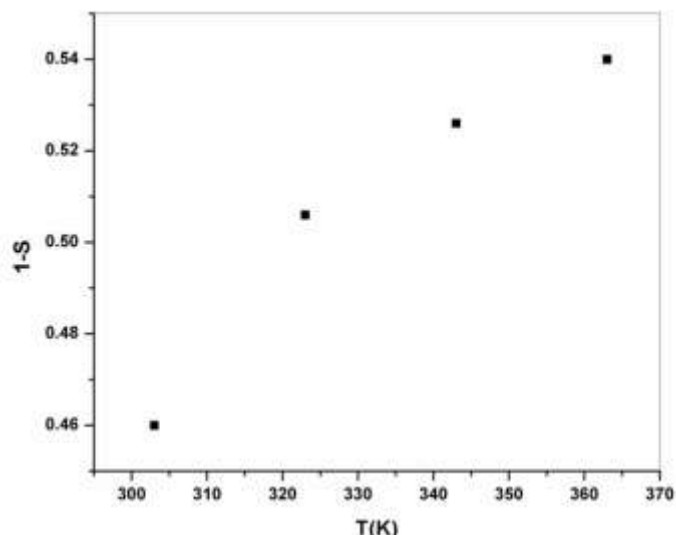


Fig. 9. Temperature dependence of (1-s) of  $\text{Co}_{0.5}\text{Zn}_{0.5}\text{Fe}_2\text{O}_4$  disk at different temperature.

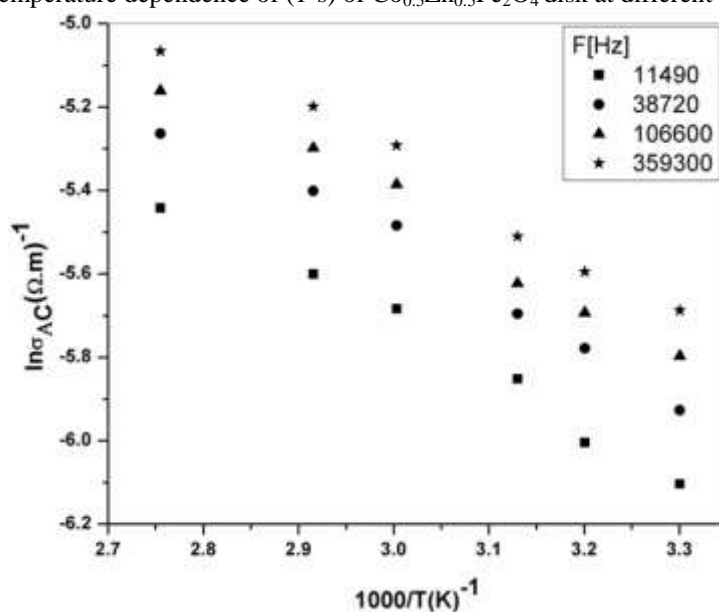


Fig. 10. Temperature dependence of AC conductivity at different frequencies for  $\text{Co}_{0.5}\text{Zn}_{0.5}\text{Fe}_2\text{O}_4$  disk.

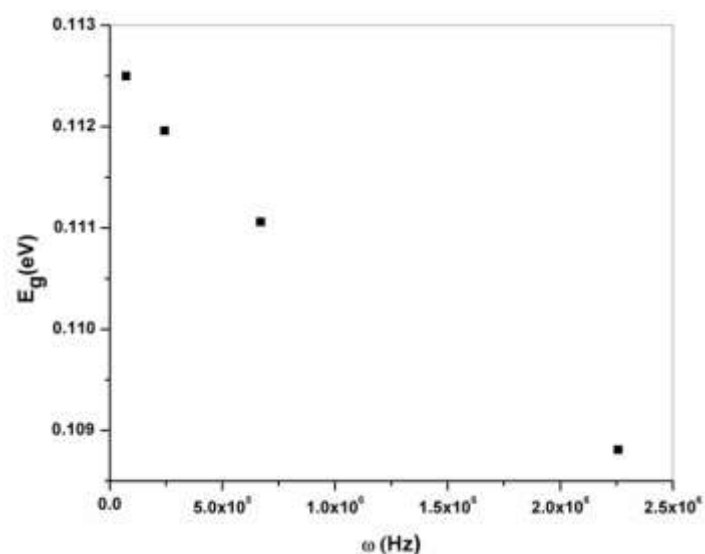


Fig. 11. Frequency dependence of activation energy for  $\text{Co}_{0.5}\text{Zn}_{0.5}\text{Fe}_2\text{O}_4$  disk.

The dependence of the real part of dielectric constant  $\epsilon'(\omega)$  on the frequency of  $\text{Co}_{0.5}\text{Zn}_{0.5}\text{Fe}_2\text{O}_4$  disk is shown at fig.12. It is clear that  $\epsilon'$  decreases with increasing frequencies, at low frequencies, due to the contribution of multicomponent of polarization [19]. At high frequencies  $\epsilon'(\omega)$  approaching constant values with increasing frequencies attributed to only the interfacial polarization [20]. It is clear from fig. 12 that as temperature increase the real part of dielectric constant  $\epsilon'(\omega)$  increase over the whole applied frequencies which can be attributed to the dipoles attain complete rotational freedom, and the effect of molecular interaction energy becomes weaker which leads to increasing off  $\epsilon'$  with increasing temperature [21].

The dependence of the imaginary part of dielectric constant  $\epsilon''(\omega)$  on the frequency of  $\text{Co}_{0.5}\text{Zn}_{0.5}\text{Fe}_2\text{O}_4$  disk at different temperature is shown at fig. 13. As observed from the fig. 13 that  $\epsilon''(\omega)$  decrease with frequency at lower frequencies due to the migration of ions which the main source of the dielectric loss of the material at low frequencies [21]. The imaginary part of dielectric constant  $\epsilon''$  decreases at higher values of frequency due to the ion vibrations may be the only source of dielectric loss [22], also observed that the imaginary part of dielectric constant  $\epsilon''$  increase with increasing temperature over the whole of applied frequencies which can be attributed conduction, dipole and vibration losses all contribute to the dielectric loss [23].

The real and imaginary parts  $M'$  and  $M''$  of complex electric modulus can be calculated from  $\epsilon'$  and  $\epsilon''$  as the following [23, 24]:

$$M'(\omega) = \frac{\epsilon'}{\epsilon'^2(\omega) + \epsilon''^2(\omega)} \tag{8}$$

$$M''(\omega) = \frac{\epsilon''}{\epsilon'^2(\omega) + \epsilon''^2(\omega)} \tag{9}$$

Figs. 14 and 15 show the real and imaginary parts of complex electric modulus  $M'$  and  $M''$ . The modulus curves indicate a broadening of peaks with change in the temperature, asymmetric in peak broadening shows the spread of relaxation times with different time constant [24-26]. Fig. 16 shows the frequency dependence of AC conductivity at different temperature of  $\text{Co}_{0.5}\text{Zn}_{0.5}\text{Fe}_2\text{O}_4$  disk in range of temperatures (303-363K). It can be noticed that the AC conductivity tend to increase with increasing the frequency. It is clear also from fig.15 that the conductivity decreases with increasing the temperature over the range of temperature (363-453K). The change of the behavior of  $\text{Co}_{0.5}\text{Zn}_{0.5}\text{Fe}_2\text{O}_4$  disk is may be due to the output of waste water which is adsorbed on the material during the synthesis step [27].

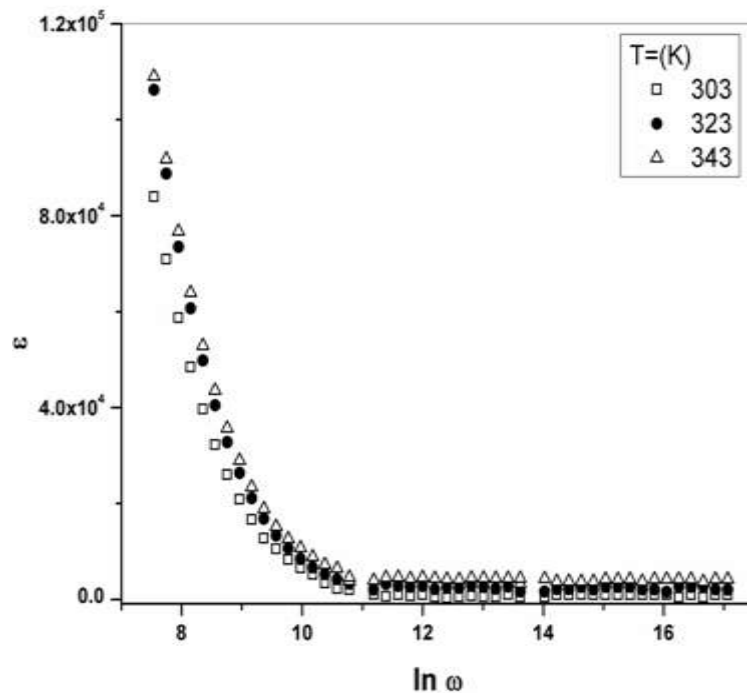


Fig. 12. the frequency dependence of  $\epsilon'(\omega)$  for  $\text{Co}_{0.5}\text{Zn}_{0.5}\text{Fe}_2\text{O}_4$  disk at different temperature.

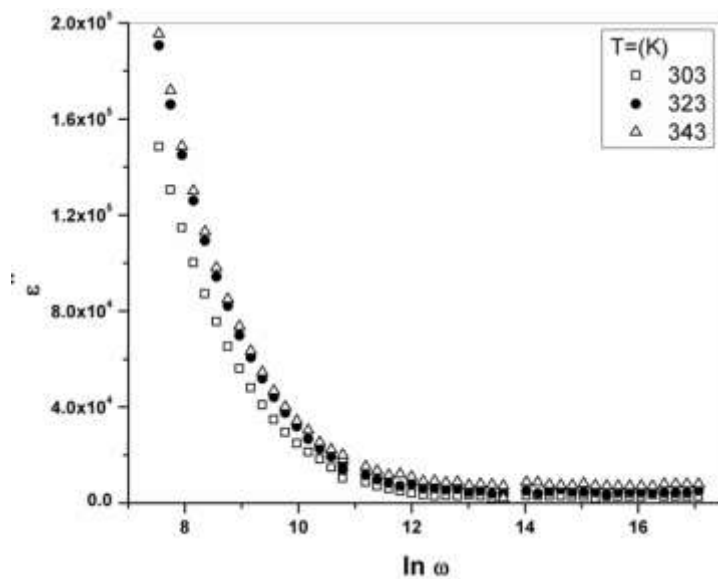


Fig. 13. The frequency dependence of  $\epsilon''(\omega)$  for  $\text{Co}_{0.5}\text{Zn}_{0.5}\text{Fe}_2\text{O}_4$  disk at different temperature.

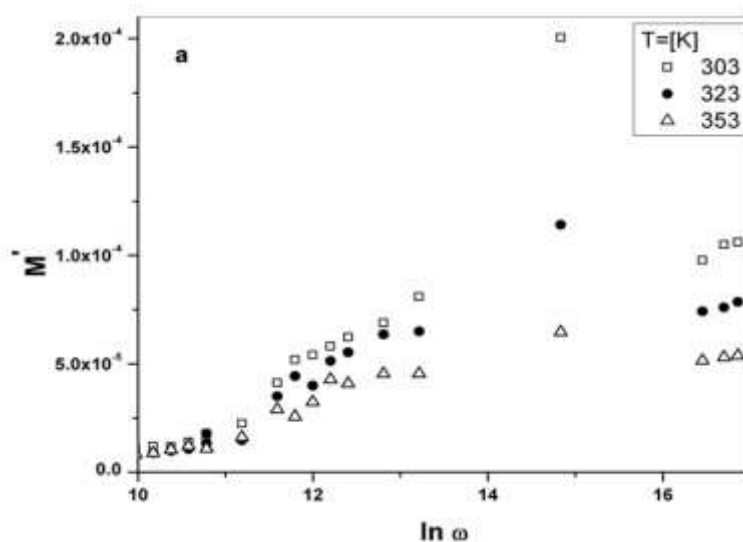


Fig. 14. the frequency dependence of the real part of the dielectric modulus,  $\epsilon'(\omega)$ , of  $\text{Co}_{0.5}\text{Zn}_{0.5}\text{Fe}_2\text{O}_4$  disk at different frequencies.

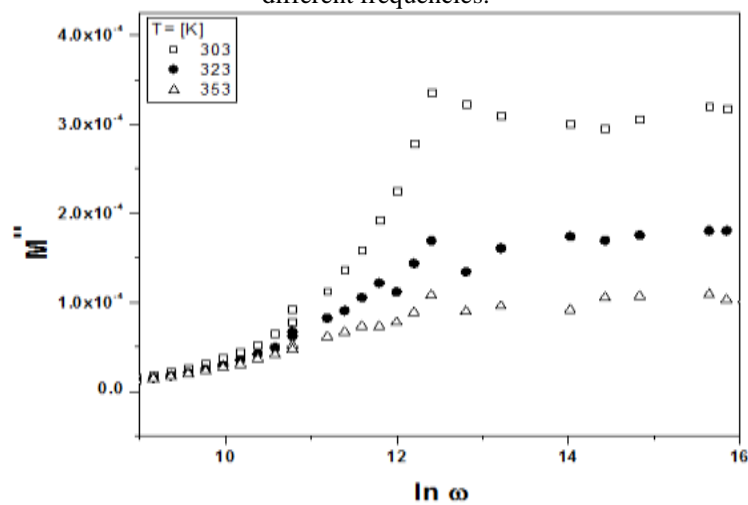
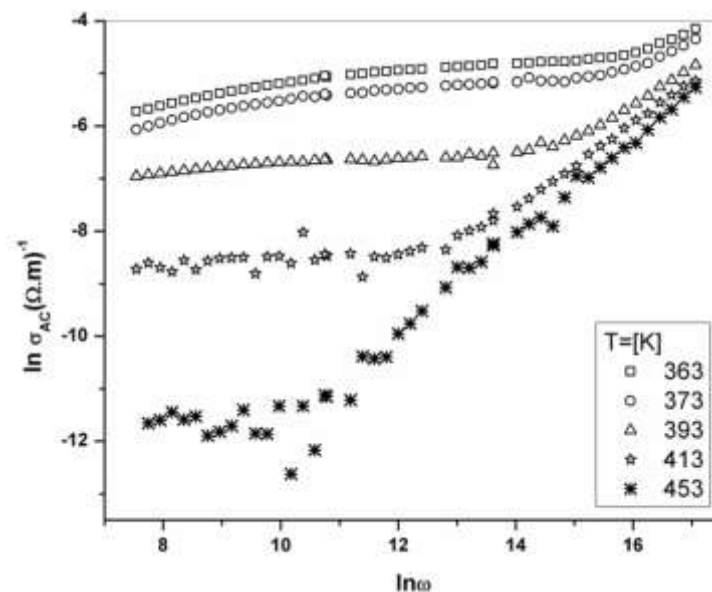


Fig. 15. the imaginary part of the dielectric modulus,  $\epsilon''(\omega)$ , of  $\text{Co}_{0.5}\text{Zn}_{0.5}\text{Fe}_2\text{O}_4$  disk at different frequencies.



**Fig. 16.** Frequency dependence of AC conductivity at different temperature of  $\text{Co}_{0.5}\text{Zn}_{0.5}\text{Fe}_2\text{O}_4$  disk in range of temperatures (363-452K).

#### IV. Conclusions

The lattice parameter for the prepared sample is much closer to the values reported for JCPDS Cards. The particle size is determined, it was found to be 11.58 nm. It is cleared that the tested particles are spherical in shape with a narrow size distribution, with a smooth surface and their particle sizes are  $9.5 \pm 2$  nm which is approximately the size calculated by both Debye–Scherrer formula and Williamsone-Hall method. The correlation barrier hopping (CBH) is considered to be the conduction mechanism in pallet of  $\text{Co}_{0.5}\text{Zn}_{0.5}\text{Fe}_2\text{O}_4$ . Activation energy was calculated at different temperature. Both dielectric loss and dielectric constant seems to decrease with the increase of the applied field. The complex dielectric modulus shows dependence on frequency.

#### References

- [1]. M.R. Bhandare., H.V. Jamadar., A.T. Pathan., B. K. Chougule., and A. M. Shaikh., Dielectric properties of Cu-substituted  $\text{Ni}_{0.5-x}\text{Zn}_{0.3}\text{Mg}_{0.2}\text{Fe}_2\text{O}_4$  ferrites, *Journal of Alloys and Compounds*, 509, 2011, pp.L113–L118.
- [2]. C.Kittel, *Introduction to Solid State Physics* (USA, John Wiley & Sons, ink, 2005)
- [3]. M. Fiebig, *J. Phys. D: Appl. Phys.*, Revival of the magnetoelectric effect, 38, 2005, R123
- [4]. N. Ponpandian, P. Balaya and A. Narayanasamy, Electrical conductivity and dielectric behaviour of nanocrystalline  $\text{NiFe}_2\text{O}_4$  spinel, *J. Phys. Condens. Matter.*, 14, 2002, 3221 – 3237
- [5]. Rani, G. Kumar, K. M. Batoor, and M. Singh, Electric and Dielectric Study of Zinc Substituted Cobalt Nanoferrites Prepared by Solution Combustion Method, *Am. J. Nanomater.*, 1 (1), 2013, 9–12.
- [6]. G. Sathishkumar, G. Sathishkumar, C. Venkataraju and K. Sivakumar, Synthesis, Structural and Dielectric Studies of Nickel Substituted Cobalt-Zinc Ferrite, *Mater. Sci. Appl.* 1, 2010, 19-24
- [7]. A. Verma, T. C. Goel, R. G. Mendiratta and M. I. Alam, Dielectric properties of NiZn ferrites prepared by the citrate precursor method, *Mater. Sci. Eng.* 60 (2) ,1999, 156-162
- [8]. H. El-Ghandoor, H.M. Zidan, Mostafa M.H. Khalil and M.I.M. Ismail, Application of laser speckle interferometry for the study of  $\text{Co}_x\text{Fe}_{(1-x)}\text{Fe}_2\text{O}_4$  magnetic fluids, *Phys. Scr.*, 86, (2012), 015403 – 015410
- [9]. H. El-Ghandoor, H.M. Zidan, Mostafa M.H. Khalil and M.I.M. Ismail, Synthesis and Some Physical Properties of Magnetite ( $\text{Fe}_3\text{O}_4$ ) Nanoparticles, *Int. J. Electrochem. Sci.*, 7, (2012), 5734 – 5745.
- [10]. A. Khorsand, W. Majid and M. Abrishami and , Ramin Yousef, X-ray analysis of ZnO nanoparticles by Williamsone-Hall and size-strain plot methods, *Solid State Sciences*, 13, 2011, 251-256
- [11]. B. Cullity and S. Stock, *Elements of X-ray Diffraction* (New Jersey, prentice-Hall, inc., 2001)
- [12]. M. Birkholz, *Thin Film Analysis by X-ray Scattering* (Wiley-VCH Verlag GmbH and Co. KGaA, Weinheim, 2006)
- [13]. V.Kumar, A. Rana, M. Yadav and R. Panta, Size-induced effect on nano-crystalline  $\text{CoFe}_2\text{O}_4$ , *J. Magn. Mater.*,320 (11), 2008, 1729-1734
- [14]. Z. T. AL-DHHAN and C. A. HOGARTH, Electrical conduction in thin films of  $\text{CeO}_2/\text{GeO}_2$ , *Journal of materials science*, 23, 1988, 2205-2212
- [15]. S. R. Elliott, A.C. Conduction in Amorphous Chalcogenide and Pnictide Semiconductors. *Advances in Physics, Advances in physics*, 36, 1987, 135-217
- [16]. S. Elliott, A theory of a.c. conduction in chalcogenide glasses, *Phil. Mag.*, 36, 1977, 1291-1304
- [17]. N. F. Mott, Conduction in glasses containing transition metal ions, *J. Non-cryst. Solids*, 1 (1), 1968, 1-17
- [18]. M. A. Afifi, A. E. Bekheet, E. Abd Elwahabb and H. E. atyia, Ac conductivity and dielectric properties of amorphous  $\text{In}_2\text{Se}_3$  films, *Vacuum*, 61, 2001, 9-17
- [19]. I. S. Yahia, N. A. Hegab, A.M. Shakra and A. M. AL-Ribaty, Conduction mechanism and the dielectric relaxation process of a- $\text{Se}_{75}\text{Te}_{25-x}\text{Ga}_x$  ( $x=0, 5, 10$  and 15 at wt %) chalcogenide glasses, *Physica B*, 407, 2012, 2476-2485

- [20]. M. M. El-Nahass, A. A. M.Faraga, F. S. H. Abu-Samah and Eman Elesh, Temperature and frequency dependencies of AC and dielectric characterizations of copper tetraphenyl porphyrin thin films, *VAC. J.*, 99, 2014, 153-159
- [21]. Sh. A. Mansour, I. S. Yahia and G.B. Sakr, Electrical conductivity and dielectric relaxation behavior of fluorescein sodium salt (FSS), *Solid State Communications*, 150, 2010, 1386-1391
- [22]. I. S. Yahia, N. A. Hegab, A. M. Shakra and A. M. AL-Ribaty, Conduction mechanism and the dielectric relaxation process of a-Se 75 Te 25- x Ga x (x= 0, 5, 10 and 15atwt%) chalcogenide glasses, *Physica B: Condensed Matter*, 407 (13), 2012, 2476-2485
- [23]. A. Oueslati, F. Hlel, K. Guidara and M. Gargouri, AC conductivity analysis and dielectric relaxation behavior of  $[N(C_3H_7)_4]_2Cu_2Cl_6$ , *J. Alloys Compd.*, 492, 2010, 508-514
- [24]. H. Smaoui, L. E. L. Mir, H. Guermazi, S. Agneland A. Toureille, Study of dielectric relaxations in zinc oxide-epoxy resin nanocomposites, *J. Alloys Compd.*, 477, 2009, 316-321
- [25]. F. S. Howell, R. A. Bose, P. B. Maced and C. T. Moynihan, Electrical Relaxation in a Glass-Forming Molten Salt, *J. Phys.Chem.*, 78, 1974, 639-648
- [26]. K. Jonscher, *Dielectric relaxation in solids* (London, Chelsea dielectric press, 1983).
- [27]. K. Praveena and K. Sadhana, Ferromagnetic Properties of Zn substituted Spinel Ferrites for High Frequency Applications, *International Journal of Scientific and Research Publications*, 5 (4), 2015, 1-21

M. I. M. Ismail "AC conductivity and dielectric properties of  $Co_{0.5}Zn_{0.5}Fe_2O_4$  nanoparticles disk" *IOSR Journal of Applied Physics (IOSR-JAP)*, Volume 9, Issue 4 Ver. 1 (Jul. – Aug. 2017), PP 57-66.